Pure appl. geophys. 165 (2008) 349–371
0033–4553/08/020349–23
DOI 10.1007/s00024-008-0300-5

Pure and Applied Geophysics

Properties of the Aftershock Sequences of the 2003 Bingöl, $M_D = 6.4$, (Turkey) Earthquake

S. Öztürk,[1] H. Çinar,[1] Y. Bayrak,[1] H. Karsli,[1] and G. Daniel[2]

Abstract—Aftershock sequences of the magnitude M_W =6.4 Bingöl earthquake of 1 May, 2003 (Turkey) are studied to analyze the spatial and temporal variability of seismicity parameters of the *b* value of the frequency-magnitude distribution and the *p* value describing the temporal decay rate of aftershocks. The catalog taken from the KOERI contains 516 events and one month's time interval. The *b* value is found as 1.49 ± 0.07 with *Mc* =3.2. Considering the error limits, *b* value is very close to the maximum *b* value stated in the literature. This larger value may be caused by the paucity of the larger aftershocks with magnitude $M_D \geq 5.0$. Also, the aftershock area is divided into four parts in order to detect the differences in *b* value and the changes illustrate the heterogeneity of the aftershock region. The *p* value is calculated as 0.86 ± 0.11, relatively small. This small *p* value may be a result of the slow decay rate of the aftershock activity and the small number of aftershocks. For the fitting of a suitable model and estimation of correct values of decay parameters, the sequence is also modeled as a background seismicty rate model. Constant background activity does not appear to be important during the first month of the Bingöl aftershock sequences and this result is coherent with an average estimation of pre-existing seismicity. The results show that usage of simple modified Omori law is reasonable for the analysis. The spatial variability in *b* value is between 1.2 and 1.8 and *p* value varies from 0.6 to 1.2. Although the physical interpretation of the spatial variability of these seismicity parameters is not straightforward, the variation of *b* and *p* values can be related to the stress and slip distribution after the mainshock, respectively. The lower *b* values are observed in the high stress regions and to a certain extent, the largest *b* values are related to Holocene alluvium. The larger *p* values are found in some part of the aftershock area although no slip occurred after the main shock and it is interpreted that this situation may be caused by the alluvium structure of the region. These results indicate that the spatial distribution in *b* and *p* values are generally related to the rupture mechanism and material properties of an aftershock area.

Key words: Bingöl earthquake, aftershock, Gutenberg-Richter relation, Omori law, constant seismicity rate model.

1. Introduction

Several authors have noted the importance of systematic investigation of aftershock sequences to earthquake prediction and a number of statistical models have been proposed to describe seismicity characters in time, space, and magnitude (e.g., Utsu,

[1] Department of Geophysics, Karadeniz Technical University, 61080 Trabzon, Turkey.
E-mail: bayrak@ktu.edu.tr
[2] Laboratoire de Géophysique Interne et Tectonophysique, Université J.Fourier, Grenoble, France.

1971; GUO and OGATA, 1997). Aftershock sequences offer a rich source of information about the Earth's crust and can provide an understanding of the mechanism of earthquakes, because literally tens of thousands of earthquakes can occur over a short period in a small area. The tectonic setting and the mode of faulting are factors other than the fault surface properties that might control the behavior of the sequences (KISSLINGER and JONES, 1991). The characteristics of sequences that may yield useful information are the spatial distribution, total number of aftershocks, and the decay rate of sequence with time. Two basic relations, the Gutenberg-Richter (G-R) law and the modified Omori law, are used to describe the aftershock activity.

The frequency-magnitude distribution (GUTENBERG and RICHTER, 1944) describes the relation between the frequency of occurrence and magnitude of earthquakes

$$\log_{10} N(M) = a - bM, \tag{1}$$

where *N(M)* is the cumulative number of events with magnitudes larger than or equal to M, a and b are constants. The parameter a showing the activity level of seismicity exhibits significant variations from region to region because it depends on the period of observations and area of investigation. The parameter b describes the size distribution of events and is related to tectonic characteristics of a region under investigation. WIEMER and KATSUMATA (1999) showed that the estimated coefficient b varies mostly from 0.6 to 1.4. Also, UTSU (1971) summarized that b-values change roughly in the range 0.3 to 2.0, depending on the different region. An estimation of the maximum b value in Gutenberg-Richter relation is achieved from empirical laws of earthquake occurrence and from dimensional considerations of power low distributions of earthquake size. The deduced maximum b values, 1.5 (or with error limits $1.30 \leq b_{\max} \leq 1.64$) agrees very well with the maximum b values computed from earthquake catalogs or published elsewhere in the literature. Thus, $b_{\max}$ is about 1.5 for intermediate and large shocks when considering the error limits. For small shocks the maximum b value may be even smaller (OLSSON, 1999). Many factors can cause perturbations of the normal b value. The b value for a region not only reflects the relative proportion of the number of large and small earthquakes in the region, but is also related to the stress condition over the region. The physical implication of the b value, however, is not as obvious.

It is well known that the decay rate of aftershock activity with time can be described using the modified Omori law (e.g., UTSU *et al.*, 1995), which can be expressed through the following equation:

$$n(t) = \frac{K}{(t+c)^p}, \tag{2}$$

where *n(t)* is the rate of occurrence of aftershocks per unit time, at time t after the main shock ($t = 0$). K, c, and p are empirically derived constants. K depends on the total number of events in the sequence, c on the rate of activity in the earliest part of the sequences. The constant c is a controversial quantity (UTSU *et al.*, 1995) and is strongly influenced by incomplete detection of small aftershocks in the early stage of the

sequences (KISSLINGER and JONES, 1991). Of these three parameters, p is a decay parameter and also the most important one. According to OLSSON (1999), p values generally vary in the interval 0.5–1.8 and this index, usually p =0.9–1.5, differs from sequence to sequence (UTSU *et al*., 1995). This variability may be related to the tectonic condition of the region, however which factor is most significant in controlling the p value is not clear.

In some cases, it is widely accepted that some time after the occurrence of a major earthquake, the aftershock activity dies off and normal, or background seismicity surpasses the aftershock activity. Therefore, seismicity rate estimations are not run with a slightly modified Omori law. For example, when p values estimations lead to low ($p < 1$) values, this could be a consequence of a strong background activity rate. In such cases, the effect of a strong background seismic activity can be misinterpreted as a slow decaying sequence. If a set of data on an aftershock sequence contains background seismicity or shocks of other aftershock sequences, it such circumstances can be taken into the model and the parameters for the aftershock sequences estimated together with the parameters for the background seismicity or the other sequences without classifying the individual shocks (UTSU *et al*., 1995). Particularly, it is added as a constant seismicity term μ to the Eq. (2) above-mentioned and written as

$$n(t) = \mu + \frac{K}{(t+c)^p}. \tag{3}$$

This modified law includes a background rate term that accounts for observed seismicity uncorrelated with any main shock. From this expression, it derives that the higher the p value, the faster the activity rate returns to its background rate value μ. Another advantage of this model is the possibility to distinguish the background rate participation in the observed aftershock rate of the Bingöl earthquake.

2. Data and Method

In this work, the aftershock sequence of the 2003 Bingöl earthquake was used to evaluate space-time-magnitude analysis. The data are taken from the website of the Bogazici University, Kandilli Observatory and Earthquake Research Institute (KOERI). The main shock ($M_W = 6.4$, $M_D = 6.4$, where M_W and M_D are moment magnitude and duration magnitude, respectively) occurred at 03:27:04 UTC on May 1 and the epicenter coordinates were determined as 39.01°N-40.47°E (KOERI). The Bingöl earthquake of 1 May, 2003 was located approximately 60 km southwest of the triple junction near Karlıova, where the North Anatolian Fault (NAF) and East Anatolian Fault (EAF) intersect. Major tectonic structures in the studied area and the vicinity are shown in Figure 1 and the faults are modified from ŞAROĞLU *et al*. (1992) and Mineral Research and Exploration of Turkey (MTA)). The NAF and EAF are the two largest strike-slip faults in Turkey, on which disastrous earthquakes occurred in historical times. According

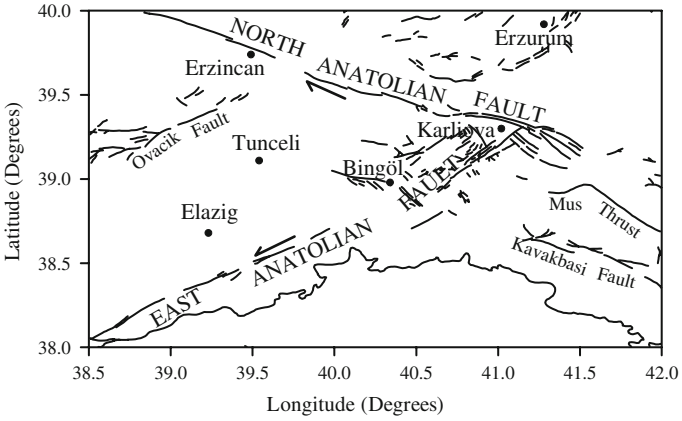

Figure 1
Major tectonic structures in and around the studied area. The most important faults such as the North Anatolian (NAF), East Anatolian (EAF), Ovacik (OVF) Faults, Mus Thrust and Kavakbasi Fault as well as some city centers are labeled.

to the fault-plane solution, as determined by the United States Geological Survey (USGS), the rupture was either left-lateral strike-slip on the EAF in a northeast-southwest direction or right-lateral strike-slip on a north-northwest trending unknown fault (MILKEREIT *et al.*, 2004). The catalog with magnitude M_D larger than or equal to 2.3 contains 516 aftershocks. This catalog is homogeneous for duration magnitude, M_{D}, and contains about one month's time period, that is, from the time of the main shock (May 1, 2003) until May 30, 2003 for the Bingöl earthquake. Figure 2 shows the hypocenters of the aftershock sequence of the Bingöl earthquake and the main tectonics of the surrounding area. It is a remarkable fact that there are no aftershocks with magnitude $M_{\mathrm{D}} \geq 5.0$. The aftershock sequence of Bingöl is completed between 2.3 and 4.6 magnitude bands. There are 20 events with magnitude $4.0 \leq M < 5.0$, and M 4.6 shock is the largest of all. Also, the depths of aftershocks are between 2.1 and 24.7 km, densely ranging 5 and 15 km. Aftershocks of the 2003 Bingöl earthquake are generally located in the Bingöl-Ağaceli-Sancak-Karakoçan region (NE-SW direction). There are numerous small faults in the aftershock region (Fig. 2). The highest density of events (all size of shocks in general) is observed in the northwest part of the main shock hypocenter (between Bingöl and Sancak). The larger events ($M \geq 4.0$) are especially observed between the main shock and Sancak. Considering the reports of Bingöl earthquake which are issued in KOERI, we used the longitudes between 40.1°E and 40.9°E, and latitudes between 38.7°N and 39.3°N as the aftershock area.

The seismological division of the KOERI determines, as rapidly and accurately as possible, the location and size of all earthquakes. Seismological Observatory of KOERI, which has computed the size of the aftershock sequence of Bingöl earthquake with $M_{D,}$ provides the real time data with the modern on-line and dial-up seismic stations in

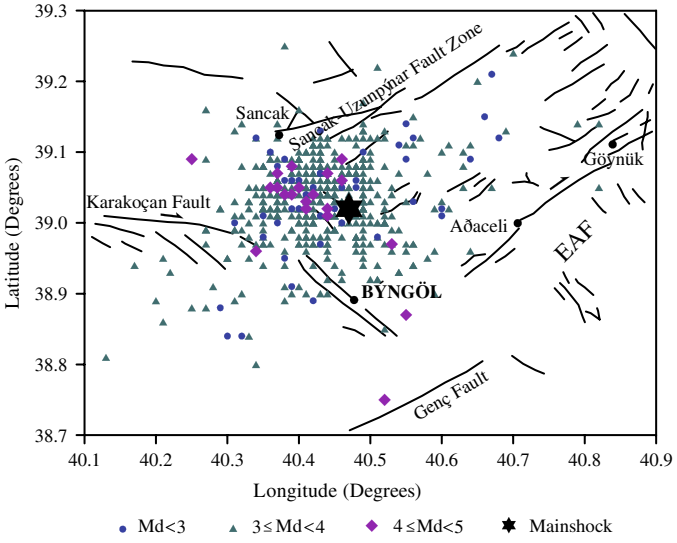

Figure 2
Epicenters of the aftershocks of the Bingöl earthquake and tectonics taken from KOERI. Data from moderate to large magnitude earthquakes are marked by different symbols and the epicenters of the main shock by stars.

Turkey. Each station is equipped with a high-gain seismometer. Signals from the stations are sent by phone lines or by radio waves to the seismological center at the KOERI. The aftershocks have been located using both analog and digital records. The errors in hypocenter distribution are about 2–3 km depending on the allocation of the stations. In this study, we did not relocate the hypocenters of aftershocks and we used the hypocenter locations of aftershocks provided by KOERI.

For the estimate of both of the *b* and *p* values, it is important to use a data set complete for all magnitude bands. The estimate of the magnitude of completeness (*Mc*) is based on the assumption of G-R power-law distribution of magnitudes. Completeness in magnitude reporting varies systematically as a function of space and time, and particularly the temporal changes can potentially produce erroneous *b* and *p* value estimates (WIEMER and KATSUMATA, 1999). Because the network may be improved after the main shock and during the first highest activity, small shocks may not be located since they fall within the coda of larger events; *Mc* will be higher in the early part of the aftershock sequence (WIEMER and KATSUMATA, 1999). The magnitude above which all events have been recorded, *Mc*, is important for all seismicity-based studies (WIEMER and WYSS, 2000) because it is frequently necessary to use the maximum number of events available for high-quality results. For the Bingöl region, we used an overlapping moving window technique (e.g., WIEMER *et al*., 1998) to compute the change of *Mc* as a function of time, starting at the main shock times. It is chosen for samples of 15 events/window to estimate *Mc*. Figure 3 shows the variations of *Mc* with time for the sequence. *Mc* is

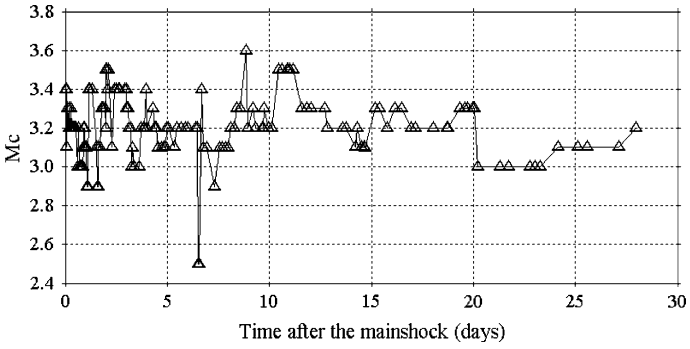

Figure 3
Magnitude of completeness, *Mc*, as a function of time for Bingöl sequence. *Mc* is computed for overlapping temporal windows, containing 15 events.

relatively high, around 3.4, at the beginning of the sequence (in the first ten hours), and then decreases to about between 3.1 and 3.3 after five days from the main shock. However, the larger *Mc* values, 3.5 and 3.6, are observed on different days, so it can be said that *Mc* generally shows a nonstable value in the sequence. In order to understand how much the *Mc* variations hinge on the sample size, we tried the different sample sizes such as 10, 25, 35 and 45 events/window for the Bingöl sequence and saw that the selection of the sample size does not effect the results. Consequently, the scatter in completeness seen in Figure 3 does not depend on the small sample size. As shown in Figure 3, *Mc* is constant about 3.2. Thus, the ZMAP program calculated the *Mc* value as 3.2 for estimating the *b* value.

Two parameters need to be adjusted in order to assure the completeness in our analysis in order to estimate the decay parameters of aftershock sequence: (1) A minimum magnitude threshold $M_{\min}$ and (2) a minimum time threshold T_{start}, i.e., excluding the first hours to days from the analysis. $M_{\min}$ would be selected for the shortest T_{start} as the most simplistic approach, and therefore the approach uses the highest *Mc* identified for the earliest part of the sequence (WIEMER and KATSUMATA, 1999). This approach, however, reduces the amount of useful data by more than one order of magnitude. For Bingöl aftershocks $M_{\min} = 3.3$ and $T_{\text{start}} = 0.01$ were chosen to determine the parameters of Omori law. Regarding *c* value (which is measured in time units, days for example) after some earthquakes, usually large ones, there is some delay (usually small) in aftershock occurrence. This can be noticed by just looking at the decay curve of aftershocks with time. However, in many cases, at the very beginning of the aftershock sequence there is a large incompleteness of the catalog, therefore an artificial high *c* value may be obtained. There is no upper limit of *c* value. However, this value is usually small or very small: for example around 0.01. By choosing $M_{\min} = 3.3$ and $T_{\text{start}} = 0.01$ for the sequence we aimed to remove these uncertainties from the estimates. In this way, even though the number of earthquakes is drastically reduced, the earliest

part of the sequence is included in the analysis and ensures completeness. Consequently, for the calculation of decay parameters of 265 events with magnitude 3.3 and larger are used which is seen in Figure 5 (a).

The *b* value in the G-R relationship is calculated by the maximum likelihood method, because it yields a more robust estimate than the least-squares regression method (AKI, 1965). The parameters in the modified Omori formula can be estimated accurately by the maximum likelihood method, assuming that the seismicity follows a nonstationary Poisson process (OGATA, 1983).

All of the computations are programmed in ZMAP (WIEMER and ZUNIGA, 1994). For spatial mapping of the frequency-magnitude distribution and the decay rate of the aftershocks, we used the gridding technique and considered the nearest epicenters, *Ne*, for each node of the grid (WIEMER and WYSS, 1997; WIEMER and KATSUMATA, 1999). The algorithm (WIEMER and WYSS, 2000) determines the minimum threshold magnitude for which the goodness of fit is greater than or equal to 95%. If there is no such magnitude for the given confidence level, a 90% goodness of fit is assigned instead. If, however, the goodness of fit is less than 90% for any threshold magnitude, the magnitude where the frequency-magnitude distribution has its maximum curvature is determined. One of these magnitudes becomes the *Mc* for that grid point. If the number of earthquakes with $M \geq Mc$ is larger than or equal to the minimum number of the nearest epicenters, $Ne_{\min}$, *b* and *p* values are computed for that node by using only the earthquakes with $M \geq Mc$. Then, spatial mapping of these parameters is plotted by the software ZMAP. Otherwise, the *b* and *p* values are not computed.

3. Statistical Assessment of the Aftershock Sequence Investigated

Figure 4 shows the frequency-magnitude relation of the Bingöl sequence. The magnitude of completeness was taken as 3.2, based on the goodness of fit of the data. ZMAP program automatically computed this magnitude value, ranging within the variation of *Mc* shown in Figure 3. Using this *Mc* value, we determined the *b* value and its standard deviation with the maximum likelihood method, as well as the *a* value of the Gutenberg-Richter relation. The *b* value is calculated as 1.49 ± 0.07 for the sequence and this value is rather large. BENDER (1983) presented a detailed analysis of the dependence of the *b* value on the interval size, maximum magnitude, sample size, and the data fitting techniques. Also, substantial errors in *b* values can be caused by incomplete catalogs, which could lead to erroneous interpretations, or the *b* values can actually increase slightly when a higher magnitude range was not included in the calculations. As stated in the data section, there are no aftershocks with magnitude $M_D \geq 5.0$ and there are only 20 aftershocks greater than *M* 4.0. Thus, this larger *b* value may result from the paucity of aftershocks whose magnitudes are larger than 5.0.

The distribution of the aftershock areas which were divided into four rectangular regions considering the *b* value spatial distribution (see Fig. 12(a)) and the variation of

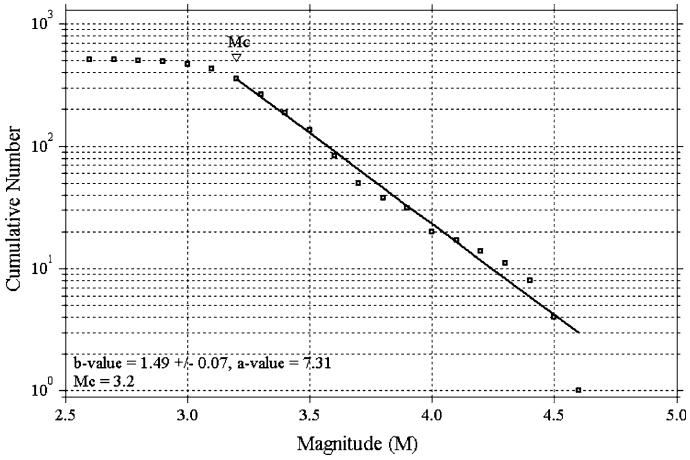

Figure 4
Frequency-magnitude distribution for Bingöl aftershocks. The *b* value and its standard deviation, as well as the *a* value in the Gutenberg-Richter relation for the sequence, are given.

the magnitude-frequency curves in these different parts of the aftershock region for detecting any significant differences in *b* value is illustrated in Figure 5. The epicenters of aftershocks with magnitudes larger than or equal to 3.3 are also depicted in Figure 5(a). For estimating the *b* values, only the shocks located inside these indicated rectangles from all events which are in Figure 2 are used. Different numbers of aftershocks and the magnitude of completeness were used in each case, due both to the variations of size of the rectangles and to the density of the seismicity in each region. The magnitude of completeness was determined with the procedure outlined above. Figure 5(b) shows the frequency-magnitude relations and *b* values of selected regions. *b* values are calculated as 1.54 ± 0.2 with $Mc = 3.4$ in region I, 1.38 ± 0.2 with $Mc = 3.2$ in region II, 1.59 ± 0.2 with $Mc = 3.2$ in region III, and 1.65 ± 0.1 with $Mc = 3.2$ in region IV, respectively. The lower *b* values are observed in the area II, while the higher *b*-values are found in the areas I, III and IV. Computations were made with 95% confidence limits (WIEMER and WYSS, 1997). Changes in the slope of the cumulative curves, namely the *b* values, can clearly be seen, illustrating the heterogeneity of the aftershock region.

Figure 6 shows the occurrence rate of the aftershock sequence of the Bingöl earthquake. As in the *b* value, the maximum likelihood procedure was used to obtain the *p*, *c* and *K* parameters and the temporal decay rate was modeled by the modified Omori formula. $p = 0.86 \pm 0.11$, relatively small, is calculated for the sequence assuming to be $M_{\min} = 3.3$, $T_{\text{start}} = 0.01$. *c* value is 0.474 ± 0.318. The small *p* values, especially for the case of a small number of aftershocks, suggest that the effect of background seismicity has not completely been removed and small *p* values have often been reported for superposed sequences. The superposed sequences consist of mostly small-sized aftershocks and a portion of these may not be real aftershocks; they may only represent

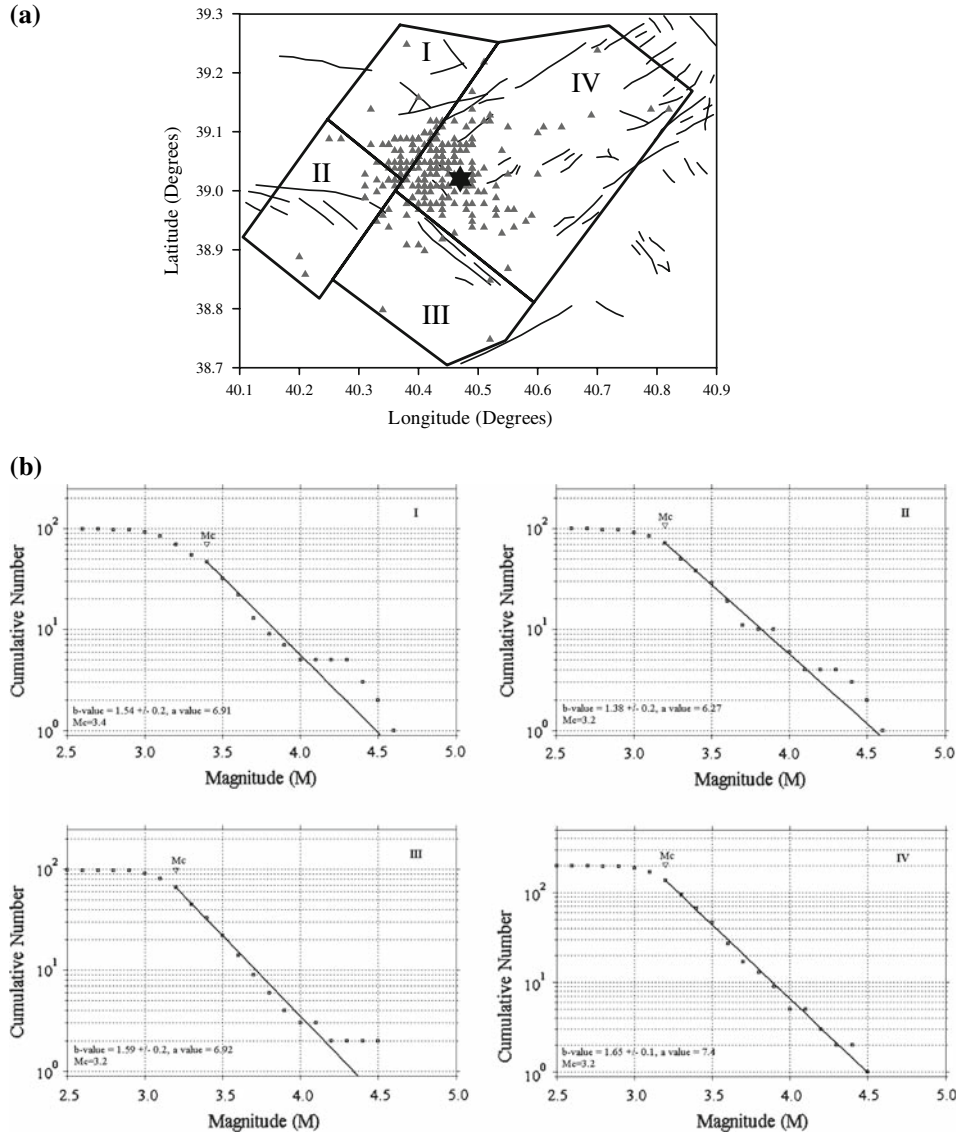

Figure 5

(a) Epicenters of the aftershocks which are labeled to identify four rectangular regions within the aftershock area, for which magnitude–frequency cumulative curves were obtained in (b). Area II coincides with the low *b*-value sections, whereas I, III and IV are marked by high *b* values. Also, this map depicts the epicenters of aftershocks with magnitudes larger than or equal to 3.3. (b) Magnitude-frequency distributions and *b* values of selected aftershock areas. Note that the number of aftershocks and the magnitude of completeness located in each rectangle are different, resulting in different estimates for the variable a value. The magnitude–frequency cumulative curves were calculated with 95% confidence limits.

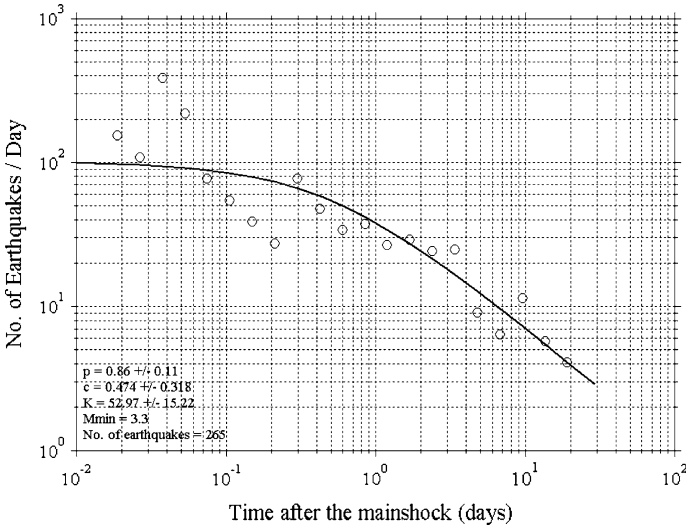

Figure 6
Decay rate of aftershock activity versus time after the main shock of Bingöl (for the cases: $M \geq 3.3$). Some relevant parameters such as *p, c* and *K* values in the modified Omori formula, the minimum magnitude for the data and the number of earthquakes are given. The data are represented by circles.

background seismicity (UTSU *et al.*, 1995). In our catalog, Bingöl sequence has 379 events, which vary between $2.5 \leq M < 3.5$. Also, the catalog consisting of whole events has 375 shocks between $0.01 \leq t \leq 10$ days, 473 shocks between $0.01 \leq t \leq 20$ days, 516 shocks between $0.01 \leq t \leq 30$ days. Considering the effects of these numbers of aftershocks, we tested the *p* and *c* values for the aftershock sequence based on the KOERI catalog. Also, for the confidence of these results we calculated *p* and *c* values according to the different number of aftershocks, time intervals, $M_{\min}$ and T_{start}. All calculations are given in Table 1. It can be clearly seen that *c* values are rather large in the first four trials and in the 7$^{\text{th}}$ trial. Conversely to high *c* values, we observed smaller *c* values in the last three trials and in the 5$^{\text{th}}$ trial. UTSU *et al.* (1995) pointed out that the *p* value is independent of $M_{\min}$, but the *c* value depends heavily on the $M_{\min}$ of the data. We tested our parameters for other $M_{\min}$ values (ranging from 2.3 to 3.4 for the sequence) and saw that the *p* value changes between 0.55 and 1.20 for different $M_{\min}$ and T_{start} but *c* value varies from 0.015 to 1.838. Eventually, it is suggested that *c* value is strongly related to the minimum magnitude in comparison with *p* value. According to the *c* values tested above is observed incompleteness at the beginning of the sequence. However, *c* value gradually increases after 20 days and this relatively large value may be caused by the incompleteness of data for later periods. There are 47 events with magnitude $M_D < 3.0$ in one month and 37 of them occurred in the first week. Thus, we can conclude that these large *c* values are due to the lack of the events smaller than *M* 3.0 after 20 days. Consequently, in our study, the calculated *c* value of 0.474 seems to be suitable for fitting

Table 1

Some calculations summing up the trials for aftershock sequence.

No	T_{start} (days)	Time interval (t, days)	M_{min}	Number of aftershocks used	p value	c value
1	0.05	-	2.3	503	1.15 ± 0.15	1.546 ± 0.683
2	0.05	-	3.3	255	1.12 ± 0.23	1.773 ± 1.179
3	0.1	-	2.3	494	1.20 ± 0.17	1.838 ± 0.848
4	0.1	-	3.3	251	1.16 ± 0.26	2.091 ± 1.450
5	-	$0.01 \leq t \leq 10$	2.3	375	0.72 ± 0.13	0.301 ± 0.240
6	-	$0.01 \leq t \leq 20$	2.3	473	0.89 ± 0.11	0.622 ± 0.328
7	-	$0.01 \leq t \leq 30$	2.3	516	1.05 ± 0.12	1.039 ± 0.436
8	-	$0.01 \leq t \leq 10$	3.3	182	0.55 ± 0.08	0.015 ± 0.038
9	-	$0.01 \leq t \leq 20$	3.3	245	0.59 ± 0.06	0.029 ± 0.047
10	-	$0.01 \leq t \leq 30$	3.3	265	0.86 ± 0.11	0.474 ± 0.318

of the aftershock sequence and in accordance with other studies. Thus, we can say that the use of $M_{min} = 3.3$, $T_{start} = 0.01$ for the calculation of decay parameters seems better to fit the sequence and the calculated relatively small p value may be a result of a small number of earthquakes.

Some seismologists are of the opinion that the number of aftershocks cannot be counted completely in the beginning of a sequence when smaller shocks are often obscured by larger ones due to overlapping, thus an overly large value of c is obtained. The value of c might be zero if all shocks could be counted (UTSU, 1971). There are two opinions concerning the c value: one is that the c value is essentially 0 and all the reported positive c values result from incompleteness in the early stage of an aftershock sequence; another is that positive c values do exist (ENESCU and ITO, 2002). If $c = 0$, *n (t)* in Eq. (2) diverges at $t = 0$. If the expansion of the aftershock area occurs in an early stage, a relatively large c value may be obtained (UTSU *et al.*, 1995). Also, for simple aftershock sequences following relatively small main shocks, estimated c values are usually small ($c \leq 0.01$ days). HIRATA (1969) found $c = 0.02$-0.5 for the 1969 Shikotan-Oki earthquake (M 6.9; from UTSU, 1969).

It is generally assumes that small p values obtained in an aftershock sequence may be caused by the background seismicity of the aftershock region. In order to perform an estimation of the best seismicity rate model, we dismissed all events with magnitude M lower than the completeness threshold $Mc = 3.3$ and we obtained 15 events between January 1, 2000 and May 1, 2003; and 266 shocks during the first month after May 1, 2003 as shown in Figure 7. We first presented an estimation of parameters from a synthetic dataset. Seismicity is seen as a nonstationary Poisson process, and model adjustment to the data is performed using a Maximum Likelihood procedure. In order to test the algorithm in charge of estimating the parameters value that best describes the data, we estimated the parameters from a synthetic dataset. Synthetics were created with parameters $K = 50$, $p = 1.1$, $c = 0.5$, $\mu = 0.1$ and $N = 266$ points, as large as Bingöl dataset (Fig. 8). From Figure 8, we clearly see that estimation of parameters with this

algorithm appears to be reliable, as the best estimate contains the true solution in its confidence intervals. However, the reader should pay attention to the importance of error within this estimate. This error is probably a consequence of adjusting a model with three free parameters (μ, c and p; K being determined optimally from the total number of aftershocks) on such a small number of aftershocks. Note also that this error provides sense of the expected lower bound on errors for mapping p values variations, as each cell of a spatial discrimination contains fewer events than the total number of aftershocks. Thus, each fit will return higher uncertainties. Also, we searched for the best parameters of Eq. (3) that describe the aftershock sequence of the Bingöl earthquake, with $Mc = 3.3$. The best fit we obtained for $\mu = 0$ (Fig. 9). Besides, the other parameters calculated in this model are compatible with the Omori model, although error in this model estimate is larger, probably because it is used for all event times, not time bins. Finally, we prepared the spatial map of μ value for the aftershock sequence as shown in Figure 10(a). It can be observed that μ parameter contribution is very weak, being estimated as 0.0 almost everywhere. This means that, even when we include a constant seismicity parameter in the seismicity rate model, it is estimated to zero. As a consequence, constant background activity does not appear to be important during the first month of the Bingöl aftershock sequence. This result is coherent with an average estimation of pre-existing seismicity, where 15 events $M > Mc$ are counted in 1215 days, leading to a weak constant rate of $\sim 12{*}10^{-3}$ days^{-1}. Furthermore, mapping variations of μ from the same model (Omori + μ) should return the results very close to these. p-value distribution obtained for the Bingöl area using a constant seismicity rate model is shown in Figure 10(b). p values are between 1.0 and 1.6, with strong spatial dependence. In addition, we do not find the same behavior for the background activity, as our estimation systematically presents a null background activity term for each point of the grid. Therefore it has no significant contribution on the aftershock decay. We argue that this feature enhances the observations of p-value variations, by suggesting variations could not be consequences of a heterogeneous background seismicity pattern. Thus, the simple modified Omori law appears reasonable to describe the occurrence decay rate in Bingöl aftershock sequence.

We also tried to fit the ETAS model to aftershock data, suggested in several studies (OGATA, 1988; UTSU *et al.*, 1995) as being a more suitable model to describe the decay of aftershock activity. The small number of events in our catalog prevented us from obtaining a reliable estimation of parameters because a multitude of earthquakes is necessary for the inversion of this model. The usage of an ETAS model that includes a constant background rate did not lead to an increase in the estimated p values. Thus, we did not use the ETAS model and switched to this Omori + constant seismicity rate model written in Eq. (3).

4. Spatial Distributions of b and p Values

For the spatial mapping of the aftershock sequence with ZMAP, we considered a spatial grid of points with a grid of 0.01°. Next, for each node the closest nearest epicenters

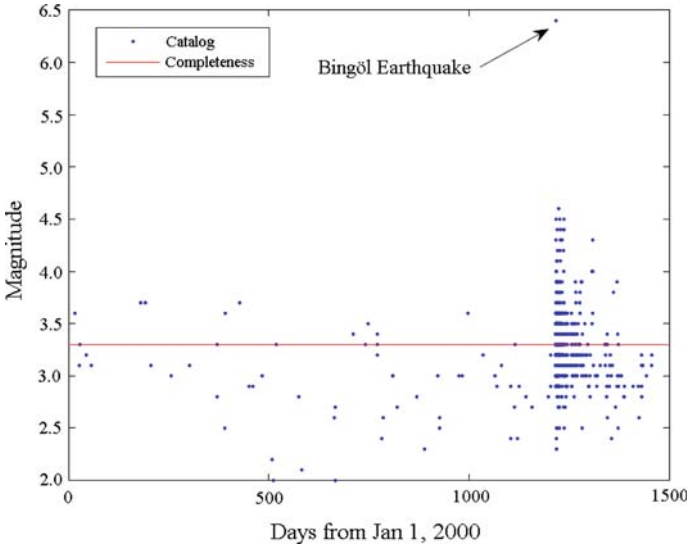

Figure 7
Time series of seismic events around the Bingöl epicenter, from January 1, 2000 to end of May 2003. Straight line indicates the completeness level set for this analysis.

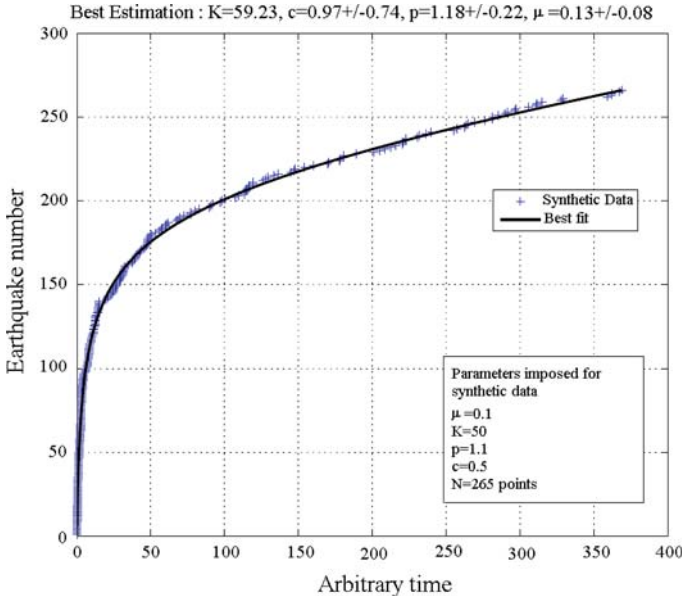

Figure 8
Estimation of parameters for a synthetic time series with $K = 50$, $p = 1.1$, $c = 0.5$ and $\mu = 0.1$ (266 points). The good agreement between synthetics and model adjustment validates the algorithm used for inversion of parameters.

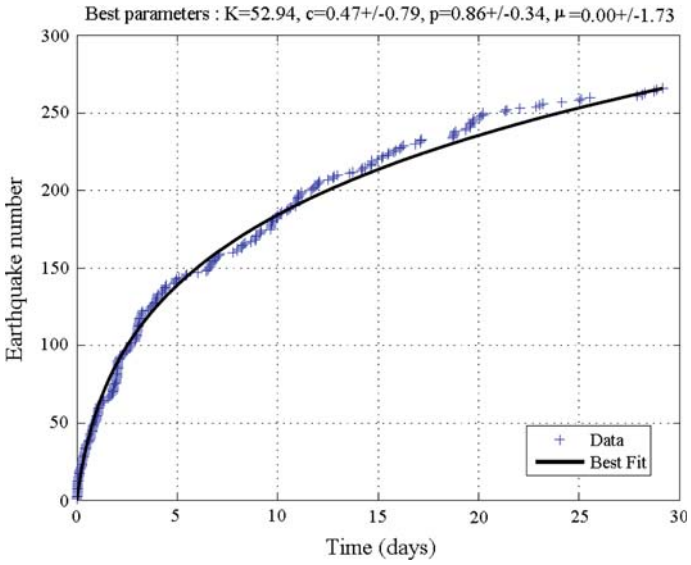

Figure 9
Estimation of parameters of aftershocks of the Bingöl earthquake according to the modified Omori law with a constant background term (first month).

(number of events) $Ne = 200$ events was considered and the minimum nearest epicenters (minimum number of events > Mc) $Ne_{\min}$ is taken as 100 for the sequence. The parameter values for nodes are represented by using a color node on the maps. One important assumption is that we chose two fixed $c = 0.474$ days, which is seen in Figure 6, in the modified Omori formula for the spatial mapping of p value, because this value is more meaningful to produce the contour maps. The magnitude of completeness varies spatially between 3.0 and 3.4, but, for most of the nodes, it has a value of 3.2 for Bingöl events. Then, ZMAP selects this minimum threshold magnitude as the Mc for all grid points and then b and p values are computed for that node by using only the earthquakes with $M \geq Mc$. Otherwise, the b and p values are not computed. Consequently, b and p values were determined using $Ne = 200$ with $Ne_{\min} = 100$ events for the sequence.

Spatial b and p value maps of sesimicity parameters for Bingöl sequence by ZMAP are shown in Figures 12(a) and (b), respectively. The spatial variations in b change from 1.2 to 1.8 and p changes between 0.6 and 1.2. Taking into consideration the b and p value alterations according to some authors (e.g., UTSU, 1971 and OLSSON, 1999), we can generally say that the b-value variations are rather large although the p value is normally distributed in the entire aftershock region. Aftershock activity of Bingöl earthquake is densely distributed around the main-shock hypocenter and the larger aftershocks are observed from the main-shock hypocenter to the NW direction. Also, the aftershocks varying between $4.0 \leq M < 5.0$ show the highest density in the NW and relatively SE parts of the main-shock hypocenter (Fig. 2). The b values can be divided into two groups: (1) lower b values (<1.4) to the NW and western part of the main shock (in the vicinity of

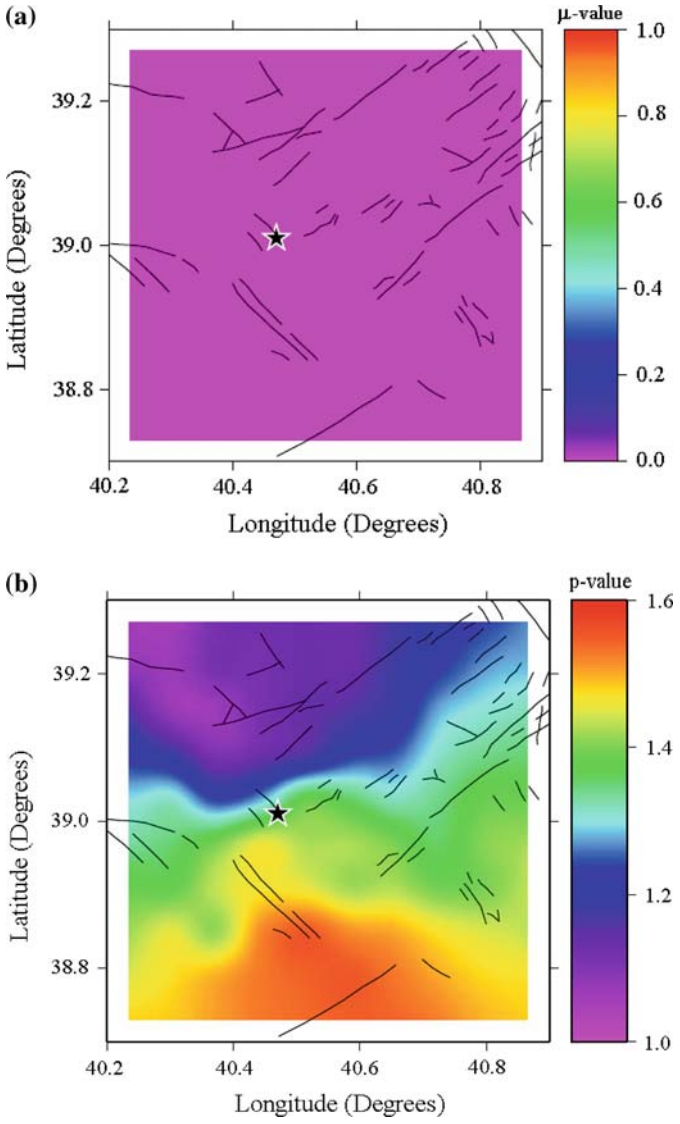

Figure 10

(a) μ-value spatial distribution for Bingöl aftershock sequence. (b) p value map for Bingöl sequence using a constant seismicity rate model based on Omori law, supplemented by a constant activity term. p value was modeled on a set of the 200 closest epicenters from each point of the grid using the earthquakes $M \geq 3.3$. Mainshock epicenter is represented by a star in (a) and (b).

Sancak and in the east of Karakoçan) and (2) higher b values (>1.6) to the eastern and NE direction from the hypocenter of the main shock. The lower b values are observed in the largest aftershock ($M \geq 4.0$) region and higher b values in the area in which less aftershock activity is observed and small shocks ($M > 4.0$) generally occurred. The p

values for Bingöl region show a tendency to decrease and are generally small in some part of the investigated area. The higher p values (>1.0) are found in the southern part of the main-shock hypocenter (between main-shock hypocenter and Bingöl) and the activity in this region shows a relatively fast decay. On the contrary, the lower p-values (<0.8) areas are found in the northern and NW part (between main-shock hypocenter and Sancak) and the moderate values (~ 0.9) in the SW (east of Karakoçan) and NE (west of Göynük) part of the sequence. The slower decay of aftershock activity to the north of the main-shock hypocenter is related to the location of strong aftershocks which is likely to generate numerous secondary aftershocks that may have lengthened the observed seismicity. This gives the appearance that decay is slower however it may actually form cascades of secondary aftershock generation processes. On the contrary, strong aftershocks to the south of the main-shock hypocenter are sparse, which leads to weaker secondary aftershock generation processes and an apparent faster-decaying seismic activity. Thus, seismic activity in the northern part of the sequence ($p \sim 0.6$) decays considerably slower than that along the southern part.

p-value distribution for Bingöl sequence, according to the background seismicity rate model, is shown in Figure 10(b). For the spatial mapping of the decay parameter, we divided the aftershock area into a grid of 10×10 nodes. For each node, the best parameters are estimated from the 200 closest events with $M \geq Mc$. The results are then interpolated between the nodes in order to produce a smoother picture of p and μ values variations, as you see on Figure 10(b). p values change between 1.0 and 1.6. The lower p values are found in the northern part of the sequence whereas the higher p values are found in the southern part. Similar distribution is generally found both in the constant seismicity rate model and simple modified Omori model. The lower and higher p values in both models are observed in the same part of the sequence, respectively. The p values calculated with ZMAP, varying between 0.6 and 1.2, are lower than those of the constant seismicity model due to background rate value μ. One can see at least two reasons for such discrepancies between the two estimates: Different spatial selection processes (for ZMAP: number of events per cell, size if individual cells or type of smoothing such as Gaussian or Kernel); or different cost function minimization schemes. Consequently, the simple modified Omori law seems to better describe the occurrence decay rate for all the periods considered in the Bingöl aftershock sequence.

5. *Discussion of the Spatial Variability of b and p Values*

The spatial and temporal variations of b and p values of an aftershock sequence have offered useful information to explain rupture mechanisms and materiel properties of an earthquake area. The variability in these values may be related to the tectonic condition of the earthquake area such as structural heterogeneity, stress, surface heat flow, and slip release, but it is not obvious which factor is most significant. In past studies, the frequency-magnitude distribution and decay rate of aftershock sequences have commonly been

simply assigned one overall value (WIEMER and KATSUMATA, 1999). A few studies, such as the one by EATON *et al*. (1970) showed the detailed spatial mapping of the frequency-magnitude distribution and *p* value for the Parkfield aftershock sequence. Subsequently, numerous studies have been done to explain spatial distribution of the *b* and *p* values in aftershock sequence. In some of these studies the distribution of *b* values has been shown to be perturbed by stress, and the relation between a lower *b* value and the higher stress after the main shock is pointed out (SCHOLZ, 1990; WIEMER and WYSS, 1997; WIEMER *et al*., 1998; ENESCU and ITO, 2002; BAYRAK and ÖZTÜRK, 2004). KISSLINGER and JONES (1991) tested the temporal behavior of 39 aftershock sequences in southern California and found no relation of *p* with either *b* value of the sequence or the main-shock magnitude. They observed *p* values varying from 0.688 to 1.809 and suggested a direct correlation between *p* value and surface heat flow. According to them, higher temperatures in the aftershock source volume caused shortened stress relaxation times in the fault zone materials, leading to a higher *p* value. According to UTSU *et al*. (1995), the heterogeneity of the crust may be related to the spatial variability of *p* value. WIEMER and WYSS (1997) hypothesized that highly stressed asperities might be defined by mapping anomalously low *b* values for different parts of the San Andreas Fault. GUO and OGATA (1997) studied 34 aftershock sequences observed in Japan from 1971 to 1995. They have proposed that the aftershock parameters for intraplate events are mainly affected by heat flow of the area or structural heterogeneity (inverse power distribution of barrier sizes), while those of interplate events are mainly affected by depth. After that, WIEMER and KATSUMATA (1999) investigated the spatial variability of *p* and *b* within one aftershock sequence for *M* 7.2 Kobe, *M* 6.2 Morgan Hill, *M* 7.2 Landers, and *M* 6.7 Northridge earthquakes. Their study is a logical extension of the work by KISSLINGER and JONES (1991) and GUO and OGATA (1997). They found for all four cases that the *b* value tends to be high near the area of the largest slip of the main-shock and frictional heat created during the event may influence the *p*-value distribution within an aftershock zone, while applied shear stress, crack density and pore pressure govern the frequency-magnitude distribution. BAYRAK and ÖZTÜRK (2004) analyzed the spatial and temporal variations of aftershock sequences of the 1999 İzmit and Düzce earthquakes. They interpreted that the variation of *b* value can be related to the stress distribution after the main shock and the larger *p* values correlate with the regions that experienced larger slip during the main shock. Also, regarding the geological aspect they concluded that the larger *b* and *p* values for two sequences are related to Holocene alluvium structures, which have low velocity. Consequently, these studies can be summarized by two hypotheses: (1) The rupture mechanisms during main shock control the spatial variations of *p* and *b* values. (2) Two parameters are dependent on the material properties of an aftershock area.

Coulomb stress changes for the area of Bingöl were calculated by STEIN *et al*. (1997), who predicted vanishing Coulomb stress changes for faults with a northwest orientation but high Coulomb stress changes southwest of Bingöl along the East Anatolian Fault. They examined the progressive failure of the North Anatolian Fault, including the Coulomb stress changes resulting from the 1971 Bingöl earthquake, in order to model the state of

stress near the triple junction of the NAF and EAF. Thus, they obtained negative Coulomb stress changes in the northwest of Bingöl. Also, NALBANT *et al.* (2002) calculated positive Coulomb stress changes along the EAF, which is located southwest of Bingöl along the EAF. However, for northwest-striking faults near Bingöl, vanishing Coulomb stress changes were modeled. Their results are in accordance with the findings of STEIN *et al.* (1997). Then, MILKEREIT *et al.* (2004) calculated Coulomb stress changes for the epicentral area of the 2003 Bingöl earthquake. According to them, the aftershocks of the 2003 Bingöl earthquake and those of the 1992 Erzincan earthquake seem to indicate the existence of a new seismically active right lateral shear zone and they showed that historical earthquakes along both the North and East Anatolian Faults led to positive changes in Coulomb failure stress for north-northwest-oriented right-lateral strike slip faults in the Bingöl epicentral area. According to the aftershock distribution of the 2003 Bingöl earthquake (see their Fig. 4), the main-shock ruptured an area of positive Coulomb stress change. Thus, they found that the earthquake took place in an area of positive Coulomb stress changes. As shown in Figure 9(a), the lowest *b* values indicating high stress changes, which is stated in STEIN *et al.* (1997) and NALBANT *et al.* (2002), are observed in the southwest direction from the main-shock hypocenter (in the east of Karakoçan). Although the stress variations around Sancak are not mentioned, low *b* values in this region are observed and we can interpret that this region may be under high stress. Also, the largest *b* values are generally related to the east and northeast parts of the main-shock hypocenter, which may have low stress and alluvium materials. As a consequence, the southwest and northwest of the main-shock hypocenter have a high stress distribution whereas there are lower stress changes in the east and northeast part of the aftershock sequence.

Geologic formation of the surrounding region is mainly composed of basalt and the basin is composed of alluvial deposits (EERI). However, due to the lack of borehole data concerning the City of Bingöl, describing the geotechnical properties of the geologic formations is not easy (ERDIK *et al.*, 2003). The geologic structure of the aftershock region is given on the website of the General Directorate of Mineral Research and Exploration (MTA) and shown in Figure 11. From the geological map, Pleistocene (local accumulations of glacial deposits, *Qe*) and Holocene (post-glacial deposits, *Qy*) alluvial fans cover the southern and eastern parts of Bingöl. The northern and western parts of Sancak show a Miocene, marine, undifferentiated formation (*md*) and neogene (the name give to the Miocene and Pliocene periods, *n*), continental, undifferentiated, respectively. Also, there are metamorphic series, undifferentiated (*Cr*) and continental, undifferentiated formations in the east and NE part of the main-shock hypocenter, respectively. BAYRAK and ÖZTÜRK (2004) found that material properties are more important factors in controlling the *b* value distributions for 1999 İzmit and Düzce earthquakes. Nonetheless the slip distribution is the most significant factor in *p* values. According to them, from the geological aspect the larger *b* and *p* values may be caused by the alluvium materials, which have low velocity. In this study, the largest *p* values (south of the main-shock hypocenter around Bingöl) are approximately observed in the Pleistocene and Holocene alluvial structures in the aftershock area whereas the largest *b* values are not exactly

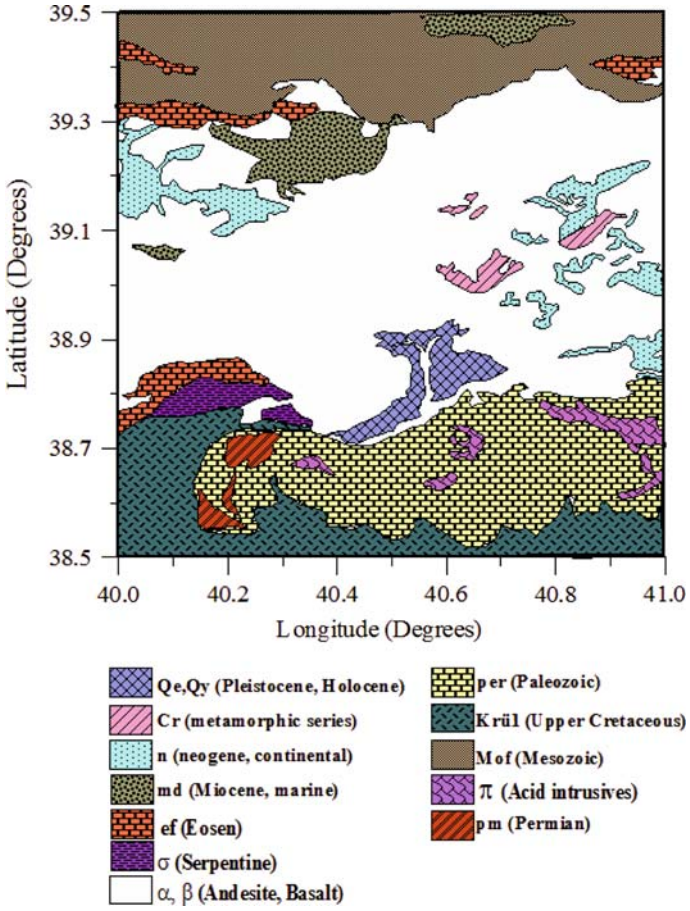

Figure 11
Surface geology in and around Bingöl. It is modified from the General Directorate of Mineral Research & Exploration (MTA) 1963.

related to the alluvium structure. EMRE *et al*. (2003) stated that no surface fractures of the causative fault have been observed in Bingöl aftershock region. Although no slip occurred in the south of the main-shock hypocenter, we observed the larger p value in this area as shown in Figure 9(b), and interpreted that this condition may be caused by the alluvium structure of the region. Thus the results in this study are consistent with the findings of BAYRAK and ÖZTÜRK (2004), to a certain extent.

6. *Conclusions*

Aftershock sequences of Bingöl earthquake which occurred in Turkey on 1 May, 2003 have been studied in order to examine their spatial and temporal properties. For this

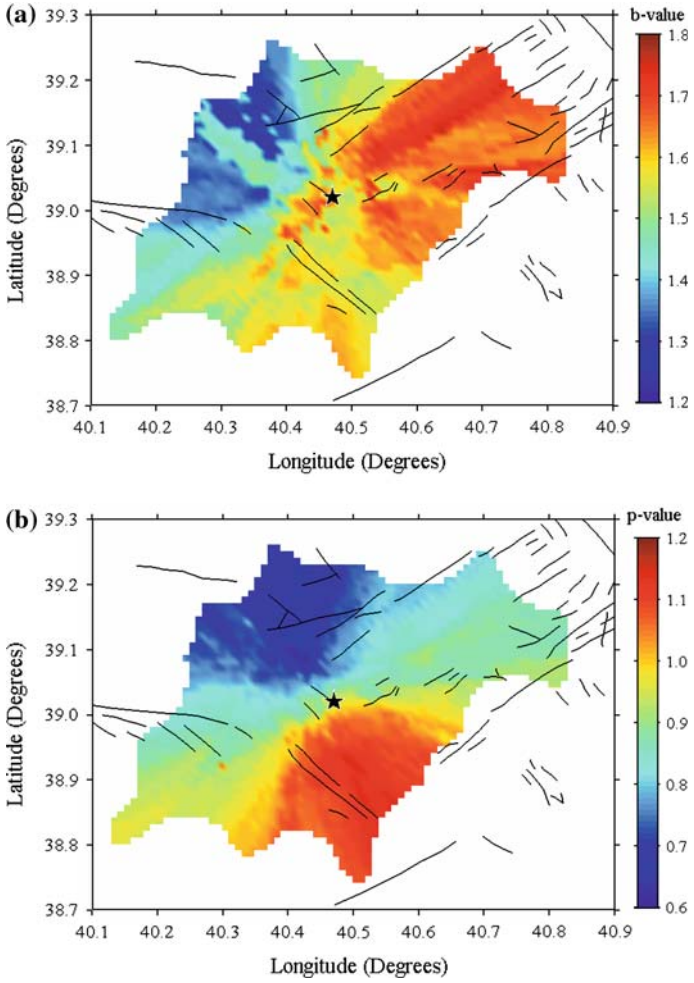

Figure 12

(a) *b*-value map for Bingöl sequence using all earthquakes $M \geq 3.3$ and $T_{start} = 0.01$. *b* value was determined by sampling the nearest 200 earthquakes for each node of a grid with nodal separation of 0.01°. (b) *p*-value map using the same grid and number of earthquakes in each grid node as in the case of *b*-value map. The values of *b* and *p* were determined using the maximum likelihood method.

purpose, the *b* and the *p* values are calculated and spatial variability in these parameters is mapped using the data containing 516 aftershocks in about one month's time interval, which is taken from the website of KOERI.

The *b* value, computed by using the events with $Mc = 3.2$, is equal to 1.49 ± 0.07. This value is very close to the maximum *b* value explained in the literature. This larger value may be connected with the error limits and the catalog, not including the aftershocks with magnitude $M_D \geq 5.0$. The magnitude interval of Bingöl sequences is

between 2.3 and 4.6 and the largest aftershock among them is 4.6, therefore these circumstances may cause a higher b value in Bingöl sequences. Also, the aftershock area is divided into four rectangular parts in order to detect the differences in b value. Changes in the slope of the cumulative curves illustrate the heterogeneity of the aftershock region.

Fitting the data for events with $M_{\min} = 3.3$, p value was obtained as 0.86 ± 0.11, relatively small, and c value 0.474 ± 0.318. Since the activity shows a relatively slow decay rate, a relatively lower p value is computed. In addition to simple modified Omori law, we calculated the decay parameters with a constant seismicity rate model in order to see a non-aftershock factor on the sequence as well as the background rate of pre-existing seismicity. μ parameter contribution leads a weak constant rate of ~ 0.012 days^{-1} for pre-existing seismicity. μ value is equal 0.0 almost everywhere for the sequence. Thus, this result is coherent with an average estimation of pre-existing seismicity. Resultingly, there is no background activity according to the parameter calculated with a constant seismicity rate model, and incompleteness at the beginning of the sequence according to the c values. However, an increase in c value after 20 days may be due to the lack of events smaller than M 3.0 at the end of 30 days. Also, p values vary from 1.0 to 1.6 according to a constant seismicity rate model, with strong spatial dependence. As in the p value variations of ZMAP, the similar distribution by constant seismicity rate model is generally calculated. The lower and higher p values in both models were observed in the same areas, respectively. Thus the simple modified Omori law appears reasonable to model the occurrence decay rate in Bingöl aftershock sequence.

The spatial variability in b value is found to change between 1.2 and 1.8. The higher b values are located in the northeast of the main-shock hypocenter while the lower b values are observed in the vicinity of Sancak and in the east of Karakoçan. The spatial variations in p value vary from 0.6 to 1.2. The p values for Bingöl region show a tendency to decrease and are rather small in some parts of the aftershock area. The higher p values are observed in the south of the main-shock hypocenter whereas the lowest p values are found in the north and northwest parts (between Sancak and the main-shock hypocenter) of the aftershock region. The lower b values are in accordance with the high stress regions. Also, the largest b values are related to Holocene alluvium materials, to a certain extent. The larger p values around Bingöl are observed although no slip occurred in this region, and we interpreted that this condition may be caused by the alluvium structure of the region. Our results suggest that the spatial variability in the parameters b and p is important and may generally reflect the rupture mechanism and the material properties of an aftershock area.

References

Aki, K. (1965), *Maximum likelihood estimate of b in the formula* $\log N = a - bM$ *and its confidence limits*, Bull. Earthquake Res. Inst., Tokyo Univ. *43*, 237–239.

BAYRAK, Y. and ÖZTÜRK, S. (2004), *Spatial and temporal variations of the aftershock sequences of the 1999 İzmit and Düzce earthquakes*, Earth Planets Space *56*, 933–944.

BENDER, B. (1983), *Maximum likelihood estimation of b values from magnitude grouped data*, Bull. Seismol. Soc. Am. *73*, 831–851.

EATON, J., O'NEIL, M., and MURDOCK, J. (1970), *Aftershocks of the 1966 Parkfield-Cholame, California, earthquake: A detailed stud*y, Bull. Seismol. Soc. Am. *60*, 1151–1197.

EERI, http://www.eeri.org/lfe/pdf/turkey_bingol_eeri_preliminary_report.pdf.

EMRE, Ö., HERECE, E., DOĞAN, A., PARLAK, O., ÖZAKSOY, V., ÇIPLAK, R., and ÖZALP, S. (2003), *May 1, 2003 Bingöl earthquake preliminary report*, MTA, Ankara.

ENESCU, B. and ITO, K. (2002), *Spatial analysis of the frequency-magnitude distribution and decay rate of aftershock activity of the 2000 Western Tottori earthquake*, Earth Planets Space *54*, 847–859.

ERDIK M., DEMIRCIOĞLU, M., BEYEN, K., SESETYAN, K., AYDINOĞLU, N., GUL, M., SIYAHI, B., ÖNEM, G., TÜZÜN, C., SALKIN, A., and KAYA, Y. (2003), *May 01, 2003 Bingöl (Turkey) earthquake, Reconnaissance Report in Turkish*, EERI.

GUO, Z. and OGATA, Y. (1997), *Statistical relation between the parameters of aftershocks in time, space, and magnitude*, J. Geophys. Res. *102*(B2), 2857–2873.

GUTENBERG, R. and RICHTER, C. F. (1944), *Frequency of earthquakes in California*, Bull. Seismol. Soc. Am. *34*, 185–188.

HIRATA, T. (1969), *Aftershock sequence of the earthquake off Shikotan Island on January 29, 1968*, Geophys. Bull. Hokkaido Univ. *21*, 33–43.

KISSLINGER, C. and JONES, L. M. (1991), *Properties of aftershock sequences in Southern California*, J. Geophys. Res. *96*(B7), 11,947–11,958.

MILKEREIT, C., GROSSER, H., WANG, R., WETZEL, H. U., WOITH, H., KARAKISA, S., ZÜNBÜL, S., and ZSCHAU, J. (2004), *Implications of the 2003 Bingöl Earthquake for the interaction between the North and East Anatolian faults*, Bull. Seismol. Soc. Am. *94*, 6, 2400–2406.

MTA, http://www.mta.gov.tr/mta_web/haritalar.asp.

NALBANT, S. S., MCCLOSKEY, J., STEACY, S., and BARKA, A. A. (2002), *Stress accumulation and increase seismic risk in eastern Turkey*, Earth Planet. Sci. Lett. *195*, 291–298.

OGATA, Y. (1983), *Estimation of parameters in the modified Omori formula for aftershock frequencies by the maximum likelihood procedure*, J. Phys. Earth *31*, 115–124.

OGATA, Y. (1988), *Statistical models for earthquake occurrences and residual analysis for point processes*, J. Am. Stat. Assoc. *83*, 9–27.

OLSSON, R. (1999), *An estimation of the maximum b value in the Gutenberg-Richter relation*, Geodynamics *27*, 547–552.

SCHOLZ, C. H., *The Mechanics of Earthquakes and Faulting* (Cambridge Univ. Press, Cambridge, 1990) 439 pp.

STEIN, R. S., BARKA, A. A., and DIETERICH, J. H. (1997), *Progressive failure on the North Anatolian Fault since 1939 by earthquake stress triggering*, Geophys. J. Int. *128*, 594–604.

ŞAROĞLU, F., EMRE, O., and KUŞCU, I. (1992), *Active Fault Map of Turkey*, General Directorate of Mineral Research and Exploration, Ankara, Turkey.

UTSU, T. (1969), *Aftershocks and earthquake statistic (I): Some parameters which characterize an aftershock sequence and their interrelation*, J. Faculty Sci., Hokkaido University, Ser. *VII*, *2*, 129–195.

UTSU, T. (1971), *Aftershocks and earthquake statistic (III): Analyses of the distribution of earthquakes in magnitude, time and space with special consideration to clustering characteristics of earthquake occurrence (1)*, J. Faculty Sci., Hokkaido University, Ser. *VII* (Geophys.) *3*, 379–441.

UTSU, T., OGATA, Y., and MATSU'URA, R. S. (1995), *The centenary of the Omori formula for decay law of aftershock activity*, J. Phys. Earth *43*, 1–33.

WIEMER, S. and ZUNIGA, R. F. (1994), *ZMAP-A software package to analyze seismicity (abstarct)*, EOS Trans. AGU *75* (43), Fall Meet. Suppl., 456.

WIEMER, S. and WYSS, M. (1997), *Mapping the frequency-magnitude distribution in asperities: An improved technique to calculate recurrence times*, J. Geophys. Res. *102*, 15,115–15,128.

WIEMER, S., MCNUTT, S. R., and WYSS, M. (1998), *Temporal and three-dimensional spatial analysis of the frequency-magnitude distribution near Long Valley Caldera, California.*, Geophys. J. Int. *134*, 409–421.

WIEMER, S. and KATSUMATA, K. (1999), *Spatial variability of seismicity parameters in aftershock zones*, J. Geophys. Res. *104*(B6), 13,135–13,151.

WIEMER, S. and WYSS, M. (2000), *Minimum magnitude of completeness in earthquake catalogs: Examples from Alaska, the Western United States, and Japan*, Bull. Seismol. Soc. Am. *90*, 859–869.

(Received May 7, 2007, accepted August 6, 2007)
Published Online First: February 28, 2008